An Improved Asymmetric Hurricane Parametric Model Based on Cross-Polarization SAR Observations

Sheng Wang, Xiaofeng Yang, *Senior Member, IEEE*, Haiyan Li, Kaijun Ren, Xiaobin Yin, *Senior Member, IEEE*, Die Hu, and Yanlei Du, *Member, IEEE*

***Abstract*—Synthetic aperture radar (SAR) has been proven to be a useful tool in monitoring hurricane structure and intensity. By far, SAR is the most promising spaceborne sensor to obtain high-resolution hurricane wind field on the ocean surface. In this article, an improved asymmetric hurricane parametric (IMAHP) model has been proposed to reconstruct the asymmetric wind speed, where the high-resolution cross-polarization SAR imagery is used to determine the value of model parameters. Compared with other models, the new model can better reconstruct hurricane wind speed with a more concise model function. For verification, taking SAR-retrieved wind speed as a reference, the root-mean-square error and bias of the wind speed estimated by the IMAHP model are 1.86 m/s, 1.89 m/s for Hurricane Arthur (2014), 2.01 m/s, 1.77 m/s for Iselle (2014), and 1.99 m/s, 1.74 m/s for Norbert (2014), respectively. Finally, comparisons with airborne stepped-frequency microwave radiometer and dropwindsondes measurements show that the wind speed simulated by the IMAHP model is close to these measurements.**

***Index Terms*—Asymmetric hurricanes, cross polarization, hurricane parametric model, synthetic aperture radar (SAR).**

Manuscript received June 10, 2020; revised August 27, 2020, September 28, 2020, and November 2, 2020; accepted November 26, 2020. Date of publication December 8, 2020; date of current version January 6, 2021. This work was supported in part by the National Natural Science Foundation of China under Grant 41871268 and in part by the Open Fund of State Key Laboratory of Remote Sensing Science under Grant OFSLRSS202009. *(Corresponding author: Xiaofeng Yang.)*

Sheng Wang is with the State Key Laboratory of Remote Sensing Science, Aerospace Information Research Institute, Chinese Academy of Sciences, Beijing 100101, China, and also with the University of Chinese Academy of Sciences, Beijing 100049, China (e-mail: wangsheng@radi.ac.cn).

Xiaofeng Yang is with the State Key Laboratory of Remote Sensing Science, Aerospace Information Research Institute, Chinese Academy of Sciences, Beijing 100101, China, and also with the Key Laboratory of Earth Observation Hainan Province, Sanya 572029, China (e-mail: yangxf@radi.ac.cn).

Haiyan Li is with the Key Laboratory of Computational Geodynamics, University of Chinese Academy of Sciences, Beijing 100049, China (e-mail: lihaiyan@ucas.edu.cn).

Kaijun Ren is with the College of Meteorology and Oceanography, National University of Defense Technology, Changsha 410073, China (e-mail: renkaijun@nudt.edu.cn).

Xiaobin Yin is with Piesat Information Technology Company Ltd., Beijing 100195, China (e-mail: yinxiaobin@piesat.cn).

Die Hu is with the University of Chinese Academy of Sciences, Beijing 100049, China (e-mail: hudie@radi.ac.cn).

Yanlei Du is with the Department of Electronic Engineering, Tsinghua University, Beijing 100084, China (e-mail: duyl01@radi.ac.cn).

Digital Object Identifier 10.1109/JSTARS.2020.3043246

I. Introduction

THE mathematical simulation of hurricanes is a widely accepted approach for estimating wind speed to design structures and assess hurricane risk [1], [2]. Generally, parametric models are the abstract description of the hurricane meteorological system using some physically meaningful parameters, such as the maximum wind speed, which represents the intensity of hurricanes and the parameter B in Holland (1980) model [3], which represents the shape of hurricanes. Also, parametric models assist in the analysis of ocean waves, storm surges, and risk assessment.

The study of parametric models relies on the support of various observation data. In the past, it was difficult to determine the inner core and surface wind field structure of hurricanes by using the flight-level aircraft reconnaissance data because the asymmetric hurricane wind field is different in azimuth, but the aircraft typically travels along the radial. With the development of remote sensing technology, using radar observation to obtain typhoon wind field information has become an effective method. Synthetic aperture radar (SAR) is unique to probe the sea surface at very high resolution under extreme weather conditions [4]–[6]. Compared to the remotely sensed winds derived by microwave scatterometer or radiometer observations, the SAR-derived wind product usually has a much higher spatial resolution to obtain the detailed distribution of hurricane winds, which is useful for capturing the structural characteristics of hurricanes, such as the eye and eyewall [7]–[9]. Using the relationship between normalized radar cross section (NRCS) and hurricanes wind speed, the 2-D sea surface wind speed can be obtained, and researchers initially proposed some geophysical model functions (GMFs) to retrieve hurricane wind speed [10]–[13]. However, the measurements of NRCS in copolarization are generally saturated under the hurricane forced wind [14], [15] Recently, studies have shown that the cross-polarized sea surface backscattering signals appear to monotonically increase with wind speed, with no dependence on wind direction and no or little dependence on radar incidence angle. Based on these new findings, several cross-polarized empirical GMFs have been established [16]–[23]. When coanalyzed with airborne stepped frequency microwave radiometer (SFMR) wind estimates, the radar backscatter signals acquired in major hurricanes from SAR reveal high sensitivity in the cross-polarized channel for wind

speeds up to 75 m/s [6]. This makes the cross-polarization SAR a unique tool in hurricane monitoring.

Using parametric models to estimate the hurricane field has become an important method in recent years. Early studies mostly assumed hurricanes or vortices with ideal symmetrical structures. Many axisymmetric models have been established based on observations and vortex theories, such as the typical gradient wind model (henceforth H80) and its revised model [24], the modified Rankine vortex [25], and several tangential wind profile models derived from it [26]–[29] as well as other tangential wind profile models based on exponential function [31]–[33]. However, the 2-D wind speed distributions simulated by these radial wind models are all axisymmetric. Nevertheless, hurricanes are rarely ideal symmetrical structures because of many factors, including friction [34], hurricane movement, vertical shear, environmental conditions [35]–[37], the near discontinuity of the surface friction and the latent heat flux [38], and the β effect [39]. In fact, the asymmetry of the wind field in azimuth is widespread. Highly asymmetric structures in a landfalling hurricane often lead to large errors in storm surge forecasting [40]. Therefore, establishing asymmetric models to estimate hurricane winds has become a difficulty and hot topic in hurricane modeling.

However, the previous asymmetric models have some shortcomings. Take the asymmetric model that introduces azimuth to describe wind speed (henceforth X06) [41] and the model based on the first azimuthal mode of asymmetry (henceforth OLF17) [42], [43] as examples; both of them have been verified to be able to describe the asymmetric characteristics of hurricanes. However, their model functions are complicated, and the determination of model parameters depends on a large number of observations. Specifically, to describe the azimuth asymmetry of maximum wind speed radius in X06 model, a fifth-order polynomial is introduced, and the determination of coefficients depends on *in situ* buoy measurements. Moreover, for the OLF17 model [refer to (2)–(4)], besides the center pressure P_c, ambient pressure P_n and shape parameters B, the parameters R_a and D that, respectively, related to the radius of maximum wind speed and shape parameters need to be determined. Among the above parameters, P_n, B, R_a, and D are determined within a reference range [43], making the accuracy of simulation results difficult to guarantee.

In this article, an improved asymmetric hurricane parametric (IMAHP) model has been proposed to estimate 2-D wind speed, and the high-resolution cross-polarized SAR data are used to determine the value of model parameters. The new model is mainly composed of two parts: 1) the tangential wind profile model proposed in [33] (henceforth M16) and 2) the improved azimuth asymmetry distribution mode (ASD) based on the M16 model. There are two main reasons for choosing the M16 model: 1) it has a relatively concise form of model function and directly uses the maximum wind speed as a model parameter to describe the hurricane intensity and 2) compared with the models based on Rankine vortex [26]–[28], it can overcome the wind speed profile's unsmooth transition in the high wind speed area (near the eyewall), which makes the model simulation results consistent with the actual change of wind speed.

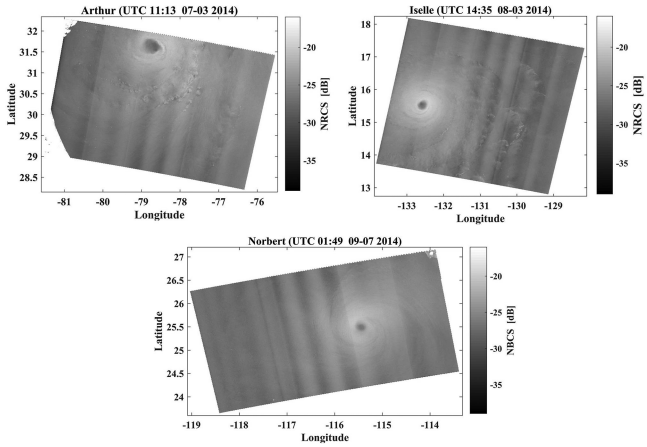

Fig. 1. Hurricanes covered by RADARSAT-2 cross- polarization ScanSAR images in 2014. RADARSAT-2 data and Products MacDonald, Dettwiler and Associates Ltd., (2008–2009).

The remainder of the article is organized as follows. The datasets are introduced in Section II. Then, the process of establishing the IMAHP model is represented in Section III. The results simulated by the IMAHP model and model assessment are shown in Section IV. Finally, the discussion and conclusion are given in Sections V and VI, respectively.

II. Dataset

A. Cross-Polarization SAR Data

In this study, three C-band RADASAT-2 cross-polarization (VH) ScanSAR wide images are used (see Fig. 1), covering three hurricanes in 2014: Norbert (01:48 UTC, September 7), Iselle (14:35 UTC, August 3), and Arthur (11:14 UTC, July 3). They are used to derive the 2-D wind speed maps and determine the value of parameters in the IMAHP model. The wind speed derived by SAR images is used as a reference for the model evaluation. The ScanSAR imaging mode provides large swaths with a width of 500 km covering areas, and the incidence angle range from 20° to 49°, with a medium resolution of 50 m. In this study, these SAR images have been calibrated and the spatial resolution has been averaged to 1 km, and before the wind retrieval from SAR images, the reference noise has been removed [18]. Then, the cross-polarization SAR wind speed retrieval algorithm, C-band cross-polarization coupled-parameters ocean (C-3PO) [21] is used to derive the 2-D wind speed with these SAR images.

B. SFMR Data

The SFMR onboard the National Oceanic and Atmospheric Administration (NOAA) WP-3D and U.S. Air Force aircraft is an airborne remote sensing instrument for measuring surface winds in hurricanes [44]. The SFMR observes TC at six frequencies, 4.55, 5.06, 5.64, 6.34, 6.96, and 7.22 GHz, and it provides along-track wind measurements up to 70 m/s [45] with relatively high spatial ($\sim$120 m) and temporal (1 Hz) resolutions. Using the latest microwave emissivity–wind speed model, the RMSE was

approximately 4 m/s between the SFMR wind speeds and the global positioning system (GPS) dropwindsonde measurements for wind speeds ranging from 10 to 70 m/s [45]. In this article, we select the SAR image of Hurricane Earl (22:59 UTC, September 2, 2010) with corresponding SFMR measurements for the case of validation with the 20-min window, from 23:00 to 23:20 UTC, September 2, 2010.

C. Dropwindsonde Data

The dropwindsonde is an expendable weather reconnaissance device developed by the National Center for Atmospheric Research (NCAR), the NOAA, and the German Aerospace Research Establishment [46]. It is designed to be dropped from an aircraft at altitude over water to measure storm conditions as the device falls to the surface. The sonde contains a GPS receiver, along with pressure, temperature, and humidity sensors to capture atmospheric profiles and thermodynamic data. The near-surface fall speed of a dropwindsonde is about 12–14 m/s, while the typical sampling rate is 2 Hz, yielding an approximately 5–7 m vertical sampling. The accuracy of the horizontal wind speed measurements is of the order of 0.5 m/s. The dropwindsonde data obtained after 2005 have been postprocessed using the ASPEN software (National Center for Atmospheric Research Atmospheric Sounding Processing Environment) [47]. Recent studies have indicated little difference between winds processed by different processing systems [48].

D. H*Wind Data

The H*Wind analysis system can be used to obtain relatively reliable wind field information, including the wind speed, wind direction, maximum wind speed and its corresponding azimuth, and hurricane central pressure [49]. This system analyzes hurricane systems and obtains wind field information by evaluating almost all available observations, which are provided by ships, buoys, coastal platforms, surface-aviation reports, and remote sensing sensors. All data are quality controlled and then processed to conform to a common framework for a 1-min sustained-wind field at a 10-m height above the sea surface [49]. The hurricane winds' errors in an H*Wind analysis are estimated to be 10%–20% [40]. Note that the wind field information provided by this system is obtained through the analysis of all available data over a period of time (e.g., 3 h). Therefore, compared with the hurricane observations at a particular time, the analysis results may be more erroneous, but this result is the best one of the overall analysis in this period. This study selected 561 H*Wind data of 42 hurricanes between 2003 and 2013 to analyze the value distribution of the asymmetric factor ε in the IMAHP model.

III. Methodology

A. Hurricane Tangential Wind Profile Model

On the one hand, the tangential wind profile model used in OLF17 model is H80 model, which is described as

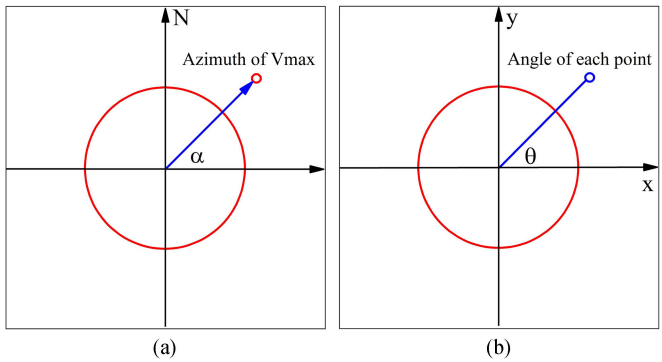

Fig. 2. Different definitions of α and θ. (a) α is defined in the geographic coordinates. (b) θ is defined in the Cartesian coordinates.

$$V_{H80} = \left[\frac{B}{\rho}\left(P_n - P_c\right)\left(\frac{R_{\max}}{r}\right)^B \exp\left(-\left(\frac{R_{\max}}{r}\right)^D\right) + \left(\frac{rf}{2}\right)^{1/2}\right]^{1/2} - \frac{rf}{2} \tag{1}$$

where P_n and P_c represent the ambient and center pressure, the parameter ρ is the air density, $R_{\max}$ is the radius at maximum wind speed, and B is the shape parameter. The parameter f is the Coriolis parameter, which can be neglected in low latitudes. It can be seen from (1) that the form of H80 model function is relatively complex. On the other hand, the concise model function of M16 is written in the form of

$$V\left(r\right) = V_{\max}\left(\frac{2R_{\max}r}{R_{\max}^2 + r^2}\right)^q \tag{2}$$

where $V_{\max}$ is the maximum wind speed, the exponent $q = 0.6$ in the original M16 model is determined for the Hudhud cyclone in the Bay of Bengal [33]. In this study, considering the different intensity and size of hurricanes in different sea areas, the value of q is not constant as in previous studies but determined according to different hurricane cases.

B. Improved Asymmetric Hurricane Parametric Model

One form of the asymmetry model has been given in [29], which is

$$V\left(r,\ \theta\right) = V_r\left(r\right) + \varepsilon V^t\left(r\right)\sin\left(\theta + \alpha\right) \tag{3}$$

where $V(r,\ \theta)$ is the asymmetric wind speed, $\mathrm{V}_r(\mathrm{r})$ is the wind speed from radial model, and $\mathrm{V}^{\mathrm{t}}(\mathrm{r})$ is the radial distribution of wind speed for the first mode of asymmetry proposed in [28]

$$V^t\left(r\right) = \varepsilon\bar{V}_{R_{\max}}\sin\left(\theta+\alpha\right)\left[e\left(\frac{R_a}{r}\right)^D exp\left(-\left(\frac{R_a}{r}\right)^D\right)\right]^{1/2} \tag{4}$$

where $\bar{V}_{R_{\max}}$ is the azimuthal average of the wind speed at $R_{\max}$ in all azimuth. ε is a factor that describes the degree of azimuthal asymmetry, which can be calculated with $\varepsilon \approx \frac{V_{\max}}{V_{R_{\max}}} - 1$. α controls the azimuth of the location of maximum wind speed [see Fig. 2(a)] and θ is the angle for each point with respect

to the horizontal axis [see Fig. 2(b)]. R_a and D are the actual location of maximum wind and sharpness of the wind field for the first mode of asymmetry, respectively. Finally, the OLF17 model function consists of the H80 model and ASD mode is

$$V_{OLF} = V_{H80}(1 + \varepsilon \sin(\theta + \alpha)\left[\left(\frac{R_a}{r}\right)^D \left(\frac{R_{\max}}{r}\right)^{-B} \exp\left(\left(\frac{R_{\max}}{r}\right)^B - \left(\frac{R_a}{r}\right)^D\right)\right]^{1/2}. \quad (5)$$

As for the OLF17 model, R_a and D are estimated by optimizing the goodness of fit criteria in the range [$R_{\max}$, 10 $R_{\max}$] and [B, 10 B], respectively. For 95% cases, R_a is generally between $R_{\max}$ and 1.2 $R_{\max}$, which means the actual location of maximum wind (R_a) is usually close to $R_{\max}$ [43]. In this article, we use the azimuth-mean winds to determine parameters related to radial winds [28], [47]; the obtained $R_{\max}$ and B represent the actual location of maximum wind and sharp parameter, which means we can set $R_a = R_{\max}$ and $D = B$. Therefore, (5) can be simplified as

$$V_{OLF} = V_{H80} + V_{H80}\varepsilon \sin(\theta + \alpha). \quad (6)$$

Then, comparing (3) and (6), we can know that $V^t(r)$ and $V_r(\mathrm{r})$ can be set to the same tangential wind profile model. Therefore, we can simplify the form of asymmetric parametric model shown in (3) into following equation:

$$V_{AM} = V_{TW} + V_{TW}\varepsilon \sin(\theta + \alpha) \quad (7)$$

where V_{AM} represents the wind speed of the asymmetric model and V_{TW} is the tangential wind speed. Note that the two terms in (7) exactly represent two parts of the asymmetric model, V_{TW} represents the axisymmetric tangential wind model, and the latter term represents the asymmetry distribution mode (ASD). In this study, we choose the M16 model as the tangential wind profile model to build an IMAHP model, which can be described as

$$V = V_{M16} + V_{M16}\varepsilon \sin(\theta + \alpha) \quad (8)$$

where V is the wind speed estimated by the IMAHP model and V_{M16} represents the tangential winds simulated by the M16 model.

IV. Results

A. Parameter Determination

Using the high-resolution cross-polarized SAR image, model parameters can be determined by the following process. First, the SAR images are resampled to 1 km to suppress noise. Second, the hurricane center can be determined with the method proposed in [28]. Then, the C-3PO algorithm [21] can be used to retrieve the 2-D wind speeds. Finally, the parameters related to the IMAHP model can be determined based on SAR-derived winds. To determine the parameter q in the M16 model, the azimuthal-mean wind speed profile should be calculated by averaging the wind speed in all azimuth. Then, q can be obtained by fitting the azimuthal-mean wind speed with (2). Fig. 3 shows

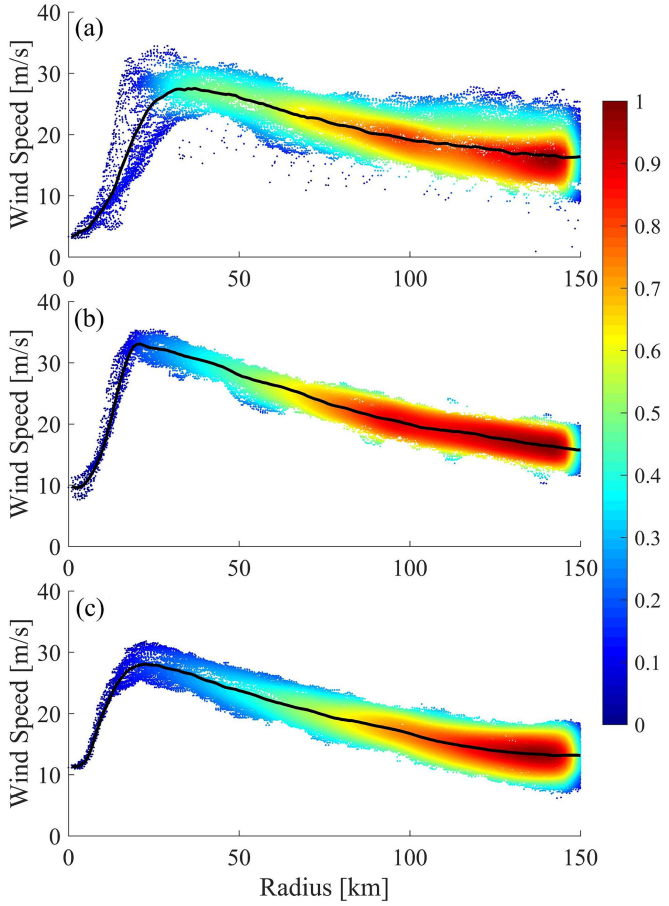

Fig. 3. SAR-derived wind speed distributions plotted as a function of hurricane radius as well as the mean wind profiles (lines in black) for three hurricanes shown in Fig. 1. The color from blue to green in the figure shows the scatter density from small to large.

the distribution of wind speed with radius derived for three hurricane cases. The black lines represent the azimuthal-mean wind speed profiles of hurricanes, and the color from blue to green in the figure shows the scatter density from small to large. As can be seen, the scatter diagram of Hurricane Iselle [see Fig. 3(b)] is the most compact, followed by Norbert [see Fig. 3(c)], and the results of Arthur [see Fig. 3(a)] are the most discrete.

Finally, the obtained values of model parameters for the three hurricanes are shown in Table I. For the three hurricanes, the order of $\varepsilon's$ values from large to small is Hurricane Arthur, Norbert, and Iselle, which is consistent with the degree of sparsity of scatter points in Fig. 3. The $R_{\max}$ in Table I has no decimal digits because the spatial resolution of SAR data has been resampled to 1 km. Besides, in order to compare the IMAHP model with the OLF17 model, the center pressure, ambient pressure, and shape parameter are needed for the OLF17 model. In this study, the center pressure data are obtained from the best track data provided by the U.S. National Hurricane Center (NHC). The ambient pressure and shape parameters are optimized in an acceptable range of [1000 hPa, 1015 hPa] and [1, 2.5] for the best fit using the RMSE as the goodness of fit criteria, respectively. Besides, for these three hurricane cases, the parameters R_a and D

TABLE I
PARAMETERS DERIVED BY THREE SAR IMAGES (2014)

Hurricane Name	Date	Time (UTC)	Hurricane Center		V_{max} (m/s)	R_{max} (km)	q	α	ε	B	P_c (hPa)	P_n (hPa)	R_a	D
			Lat	Lon										
Arthur	07-03	11:14	31.66° N	78.69° W	27.53	37	0.73	97°	0.16	1.5	981	1000	37	1.5
Iselle	08-03	14:35	15.53° N	132.60° W	33.05	21	0.60	23°	0.04	1.3	966	1000	21	1.3
Norbert	09-07	01:49	25.50° N	115.45° W	28.04	22	0.65	333°	0.11	1.3	979	1000	22	1.3

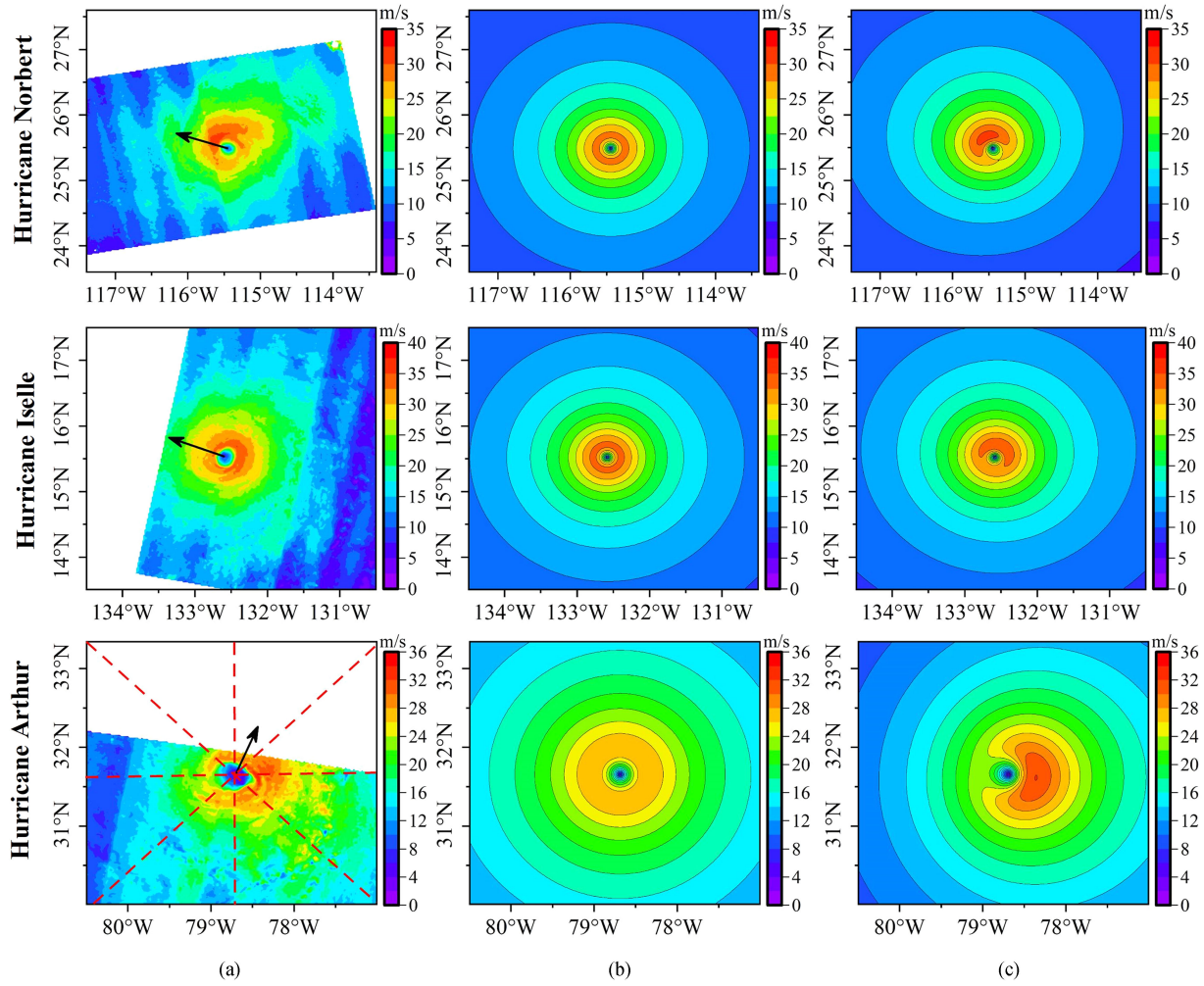

Fig. 4. Distribution of 2-D wind speed derived by SAR and models. Each row represents the wind speed of the same hurricane using different models, and each column represents the wind speed calculated by the same model. The black arrows indicate the direction of the movement of hurricanes, which are calculated from the best track data. The red dotted line in the upper left subgraph represents the position of the profiles in eight main directions. (a) SAR-derived wind speed. (b) M16 model wind speed. (c) IMAHP model wind speed.

for the OLF17 model are determined as $R_a = R_{\max}$ and $D = B$ by optimizing the goodness of fit criteria in the range mentioned in (5).

B. Comparison Between Models

Based on the model parameters extracted above, the simulated 2-D wind speed can be obtained. Fig. 4 shows the distribution of wind speed derived by SAR and simulated by models. As shown in Fig. 4 (first column), the distributions of wind speed for the three hurricanes are all asymmetric with different degrees of asymmetry. The wind speed simulated by the M16 model (second column in Fig. 4) is axis symmetrical and significantly different from the actual wind speed. For the IMAHP model (third column in Fig. 4), the estimated results fit well with the actual wind speed, which indicates that the new model can

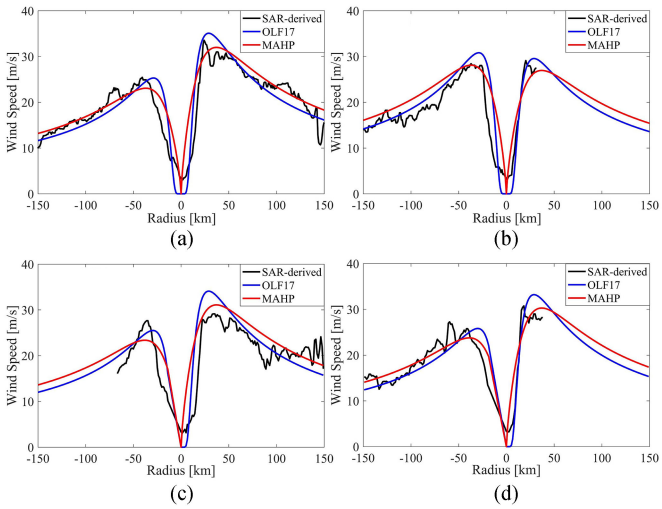

Fig. 5. Wind speed profiles in eight main directions for Hurricane Arthur. (a) E-W. (b) N-S. (c) NW-SE. (d) NE-SW.

TABLE II
STATISTICS CALCULATED BY COMPARING THE WIND SPEED DERIVED BY SAR IMAGES AND MODELS

Statistics		RMSE (m/s)	Bias (m/s)	Correlation (R^2)
Hurricane Arthur	H80	2.96	3.25	0.76
	OLF17	2.36	2.50	0.87
	M16	2.64	2.91	0.76
	MAHP	1.86	1.89	0.89
Hurricane Iselle	H80	3.11	2.95	0.92
	OLF17	3.11	2.96	0.92
	M16	2.04	1.80	0.92
	MAHP	2.01	1.77	0.92
Hurricane Norbert	H80	2.19	2.00	0.89
	OLF17	2.15	1.87	0.90
	M16	2.06	1.82	0.89
	MAHP	1.99	1.74	0.90

effectively describe the asymmetry of wind speed distribution. It should be noted that, because the ASD of the IMAHP model is based on the first azimuthal mode of asymmetry (i.e., sinusoidal function), it can only describe one high wind speed zone and its corresponding weak wind speed zone in the opposite direction. This is because the sinusoidal function has only one maximum and one minimum in a period (360°), and their corresponding angles are precisely 180° apart.

Although both the ASD modes of IMAHP and OLF17 model are based on the first azimuthal mode of asymmetry, they adopt different tangential wind profile models. It causes differences in the wind speeds simulated by these two models. To effectively evaluate the performance of the new model, we first chose four winds profiles covering the main eight directions (E-W, N-S, NW-SE, and NE-SW) in the radial direction to do the verification. Taking Hurricane Arthur, which has the largest degree of asymmetry, as an example, the position of profiles on the SAR image is marked in the lower left subgraph of Fig. 4, and their corresponding wind speed profiles are presented in Fig. 5. The results simulated by the IMAHP model are in good agreement with the SAR-derived one, which demonstrates the ability of the new model to depict the asymmetry of hurricanes. As for the comparison between models, the wind speed profiles of the IMAHP model have slightly better performance than the OLF17 model. Especially, in the east-west (E-W) direction covering the strongest and weakest wind speed regions of the hurricane, as Fig. 5(a) shows, the wind speed profile of IMAHP is significantly closer to the of SAR-derived one. However, it should be noted that both the OLF17 model and the IMAHP model are not very good at fitting in the inner region of the hurricane eye ($r < R_{\max}$). Although we can improve the simulation effect by adding parameters or adopting other tangential wind models, more parameters mean that the simplicity of the new model will be lost. Therefore, the new model presented in this article is the best choice under careful consideration.

Moreover, in order to evaluate the IMAHP model quantitatively, the statistical analysis of model estimation results has been done regarding the SAR-derived one as references, which are shown in Table II. The RMSE, bias, and correlation coefficient (R^2) for the IMAHP model are 1.86 m/s, 1.89 m/s, 0.89 for Hurricane Arthur, 2.01 m/s, 1.77 m/s, 0.92 for Iselle, and 1.99 m/s, 1.74 m/s, 0.90 for Norbert, respectively, which is significantly superior to the statistical results of the OLF17 model. As can be seen in Table II, the accuracy of the M16 model is higher than the H80 model. This is because the M16 model directly uses the maximum wind speed as a model parameter and can get more accurate information about the intensity of the hurricanes. In contrast, the H80 model describes the hurricane intensity with the difference between the central pressure (P_c) of the hurricane and the ambient pressure (P_n). The better performance in describing the radial winds of the M16 model is the main reason for the accuracy improvement of the IMAHP model. Also, it can be easily known that the greater the degree of asymmetry of hurricanes, the greater the accuracy difference between the axisymmetric model and the asymmetric model. For example, the RMSE for the M16 model and IMAHP model are 2.04 m/s, 2.01 m/s for Iselle, 2.06 m/s, 1.99 m/s for Norbert, and 2.64 m/s, 1.86 m/s for Arthur, respectively. As the degree of asymmetry (value of ε) increases, the differences in the values of RMSE between the two models are 0.03, 0.07, and 0.78 m/s, respectively. Therefore, it is easy to understand that when the hurricane's asymmetry is high, using an asymmetry model to simulate the wind speed will make a relatively large error.

Fig. 6 shows the comparison between the wind speed derived by SAR images and the IMAHP model for the three hurricanes. Except for the obvious abnormal scatter points, most data points follow a linear distribution. Specifically, most of the data are distributed in the range of 10–20 m/s. There is a good agreement between model simulations and SAR measurements for high wind speed data (>20 m/s). However, for the low wind speed data (<10 m/s), there is a relatively big gap between the model results and SAR-derived winds. An overestimation of low wind speed is presented. The reason for these outliers in Fig. 6 is that

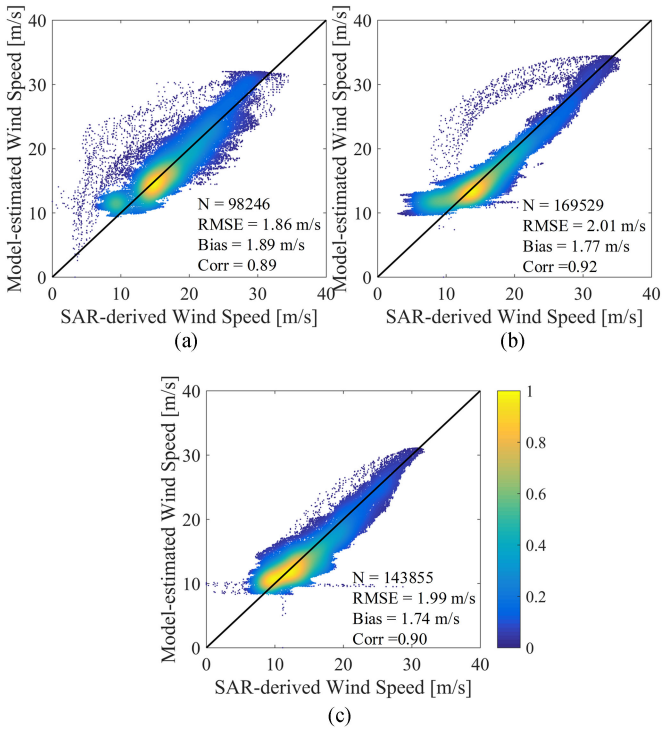

Fig. 6. Comparison between the wind speed retrieved by SAR images and simulated by IMAHP model for three hurricanes. (a) Hurricane Arthur. (b) Hurricane Iselle. (c) Hurricane Norbert.

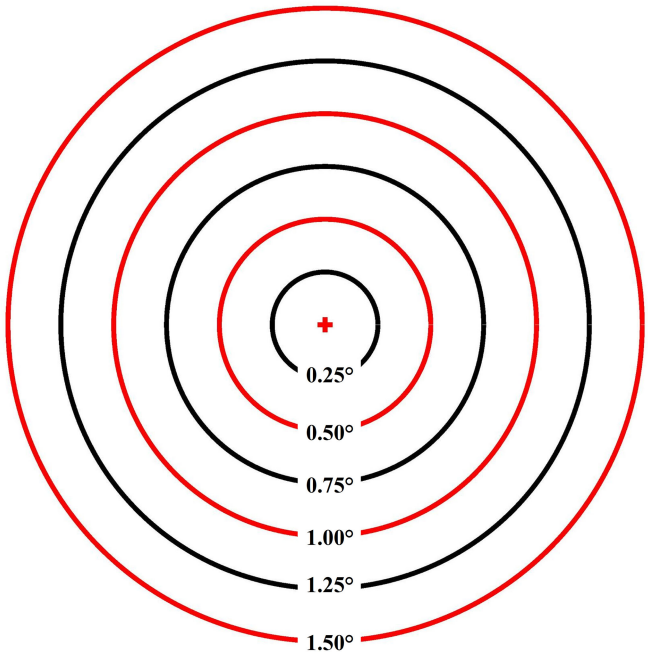

Fig. 7. Each subregion for hurricanes (0.25° interval). The red plus indicates the central position of hurricanes.

there are noise and radar beam edge areas in the SAR images, and calibration and denoising procedures cannot completely eliminate these noise effects. The overestimation of low wind speed is because the IMAHP model usually has poor performance in the hurricane eye area.

In order to quantitatively verify whether the distance from hurricane center impacts the accuracy of the models, as shown in Fig. 7, we divide the core area of hurricanes (0°–1.5°) into several annular regions at intervals of 0.25° and calculate the RMSE and bias for each annular region. The results are shown in Fig. 8, from which we can roughly divide the changing trend of RMSE and bias into three stages—declining, basically flatting, and slowly rising. The errors in the eye region (0°–0.25°) are the largest among these annular subregions, which quantitatively proves the previous conclusion that these models do not perform well in the eye region. As the distance extends to 1° (0.25°–1°), the accuracy of the models is significantly higher than that in the eye area, and the RMSE and bias are both less than 3 m/s in all annular subregions. Moreover, as the distance continues to expand outward (1°–1.5°), the values of RMSE and bias gradually increase, which means that the applicability of the models will gradually decrease in areas away from the center of the hurricanes. For the comparison among different models, the RMSE and bias of the IMAHP model are minimal in most annular subregions. Besides, for the subregions where the accuracy of the M16 model is higher than the H80 model, the accuracy of the IMAHP model is also better than that of the OLF17 model in most subregions [except two subregions in 0.5°–1.0° in Fig. 8(b)], which indicates that it is feasible to improve the asymmetric model by improving the tangential wind profile model. Whether it is a comparison for overall or subregions, the IMAHP model's accuracy is higher than that of the OLF17 model.

C. Validation With Aircraft Measurements

Hurricane Earl (2010) is selected for the verification against the aircraft measurements. Similar to previous studies, we assume the structures of the hurricanes remain steady during the ±3 h periods [28], [47]. Note that the relative positions of dropwindsondes are obtained by removing the physical radial locations of observations from the hurricane center location, which are calculated based on the linearly interpolated best track data. For the SFMR measurements, we choose one complete radial profile observation with a radial of 150 km. The track of selected SFMR measurements and the storm-relative locations of the dropwindsondes during the ±3 h of collocation time are shown in Fig. 9.

As shown in Fig. 10, the IMAHP model simulation results are in good agreement with the SFMR measurements, but there will be some differences in model performance at different distances from the hurricane center. Specifically, the IMAHP model performs well in the external wind field (larger than $R_{\max}$), but the errors are relatively large in the hurricane eye area (smaller than $R_{\max}$). By comparing the profile of wind derived by SAR image (blue line) and the profile of rain rate (brown dotted line) in Fig. 10, it is known that the heavy precipitation caused the underestimation of wind speed retrieved by SAR because heavy rain associated with a hurricane attenuates the radar signal of SAR [50]. Unfortunately, the red profile of the IMAHP model in Fig. 10 has missed the maximum wind speed. There are two main reasons for this result. First, heavy

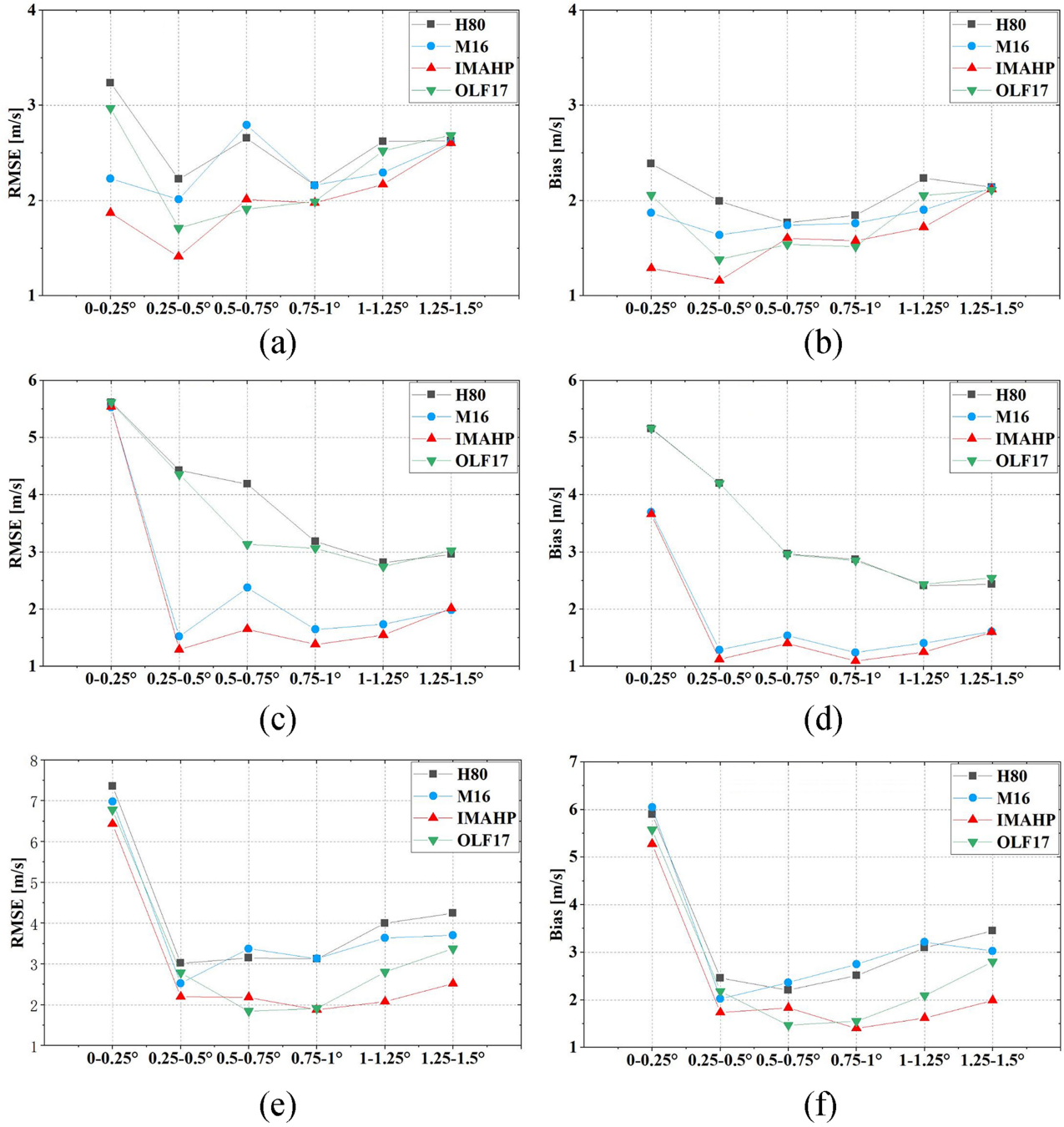

Fig. 8. RMSE and bias between the wind speed derived by SAR images and models for each circular region of hurricanes. (a) RMSE and (b) bias for Hurricane Norbert. (c) RMSE and (d) bias for Hurricane Iselle. (e) RMSE and (f) bias for Hurricane Arthur.

rain caused an underestimation of the wind speed obtained by SAR at the hurricane eyewall, which made the model parameter calculated from SAR-derived winds $V_{\max}$ lower than the actual value. Therefore, wind speeds estimated by the model are also lower than the actual wind speed at eyewall. Actually, in order to verify the model's underestimation of the high wind speed in the hurricane eyewall, we have simply compared the maximum wind speed simulated by the IMAHP model with that obtained from best track data, the model simulated results are 32.03, 34.46, 31.06, and 36.94 m/s for Arthur, Iselle, Norbert, and Earl, respectively. In comparison, those from best track are 78 knot (40.12 m/s), 100 knot (51.14 m/s), 76 knot (39.09 m/s) and 90 knot (46.30 m/s), respectively. The model simulation results are underestimated. Second, the first mode of asymmetry can only capture one strong wind region in the direction of the location of maximum wind speed. In this direction, the winds will strengthen based on the azimuth-mean wind speed, while in the opposite direction, winds will weaken. For Hurricane Earl (2010), the direction of maximum wind speed is close to the east, but the SFMR track is in the northwest, which is in the

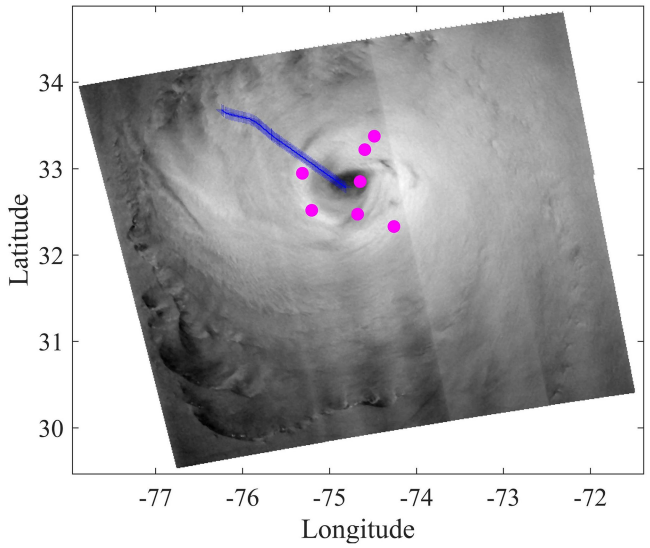

Fig. 9. RADARSAT-2 cross-polarized SAR image for Hurricane Earl (22:59 UTC, September 2, 2010). The track of SFMR (blue line) used here from 23:00 to 23:20 UTC (September 2, 2010), and the relative positions of dropwindsondes to hurricane center (points in magenta) during ±3 h of collocation time.

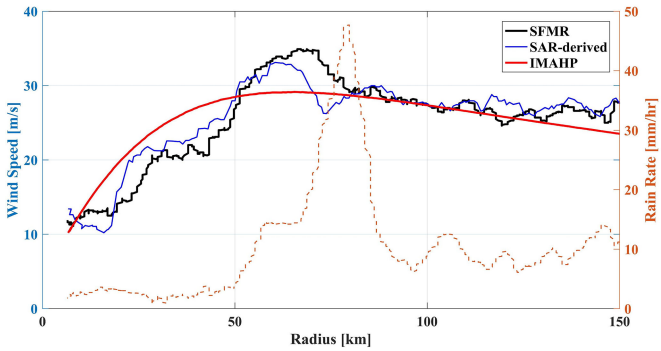

Fig. 10. Wind speed profiles measured by the SFMR (black line), estimated by the IMAHP model (red line) and retrieved by SAR images (blue line) for Hurricane Earl (22:59 UTC, September 2, 2010). The brown dotted line represents the rain rate observed by SFMR.

regions where the wind speed is low. Therefore, the IMAHP model has not captured the high winds of SFMR measurements in the opposite direction of the maximum wind speed. Even so, the maximum wind speed for this wind profile simulated by the IMAHP model (29.14 m/s) is relatively close to that of SFMR measurements (34.90 m/s) with their corresponding radii are 64 and 60.5 km, respectively.

The comparison between the wind speed observed by the collocated dropwindsondes and simulated by the IMAHP model is shown in Fig. 11. Actually, limited by the quantity and quality of dropwindsonde data for Hurricane Earl, the statistics results are not very good, which are 10.11 m/s, 4.74 m/s and 0.78 for RMSE, bias, and correlation coefficients, respectively. Suppose there are more data or better data quality, the IMAHP simulated wind speed and dropwindsondes measurements will fit better. For example, when we select Hurricane Arthur (2014) as the tested case, the statistics in terms of RMSE, bias, and correlation coefficients are 3.23 m/s, −0.69 m/s, and 0.86, respectively.

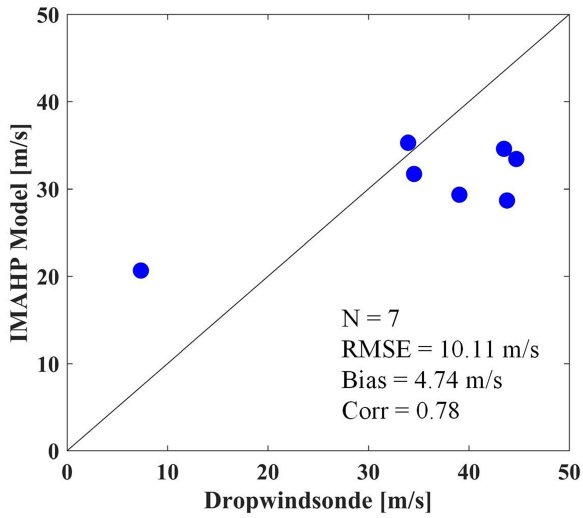

Fig. 11. Comparison between the wind speed observed by the collocated dropwindsondes and simulated by IMAHP model for Hurricane Earl (2010).

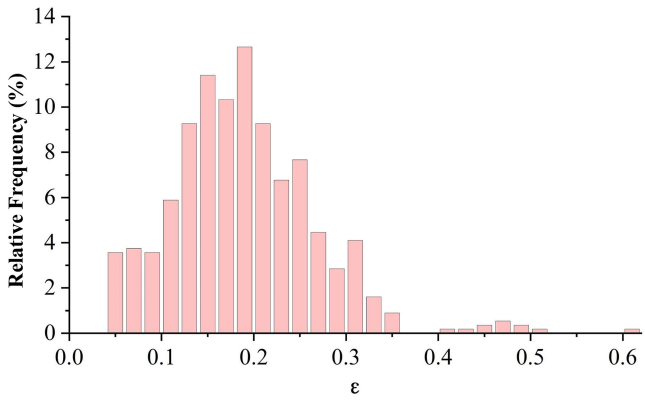

Fig. 12. Histogram for distribution of the value of ε , the dataset consists of 42 hurricanes H*Wind data between 2003 and 2013.

V. Discussion

The distribution of the value of the asymmetric factor ε has been discussed in the study of the OLF17 model [43]. The researchers used H*Wind data to calculate the asymmetric factor of six groups of hurricanes, and the results showed that about half of the asymmetric factors of hurricanes were greater than 0.12. However, due to the small amount of data involved, this conclusion has limited guiding significance for parameter ε determination. In this study, we selected 561 H*Wind data of 42 hurricanes between 2003 and 2013 to analyze the optimum values and distributions of the asymmetric distribution factor ε. It is noted that cases below hurricane strength were excluded from the selection of samples. Fig. 12 shows that the relative frequency is the highest when the value of ε is close to 0.18. On the whole, the value of ε is mainly in the range [0.04, 0.35], and in this range, the cases account for over 98% of the total. When the value of ε is greater than 0.35, the corresponding relative frequency can almost be neglected. When the value of ε is in the range [0.12, 0.22], the relative frequency of each subinterval in this range is more than 10%, and the sum of the cases accounts for about 60% of the total.

Moreover, Fig. 10 shows that the cross-polarized SAR-retrieved hurricane wind speed is relatively low. This may be caused by the heavy rain. Although the C-band radar is less influenced by rain compared with X-band and Ku-band, the signature of heavy precipitation inside cyclones can still be clearly seen in C-band SAR images. This rain-effect sometimes can contribute up to 100% error for SAR wind retrieval under hurricane conditions [51]. Recently, Shen et al. developed a scheme to label rain cells inside cyclones and correct their effects on SAR-derived winds [52]. However, the rain-corrected SAR winds still have a negative bias when comparing with SFMR winds (as shown in [52, Fig. 10A]). This reveals that the existing cross-polarization GMFs used in hurricane wind retrieval may need further improvements.

Another issue of the cross-polarization SAR wind retrieval is the noise effect (as shown in Fig. 1). Scanning SAR (ScanSAR) technique is commonly used in SAR satellite missions to obtain large swath. In the ScanSAR imaging mode, the radar periodically switches the antenna beam to several subswathes in the range direction to obtain broader coverage. In each subswath, the radar beam acquires a finite periodical sequence of echoes (so-called bursts). In each burst, the echo intensity at the edges of the antenna beam is much larger than that close to its center, which causes the "scalloping noises." Because of the relatively low signal-to-noise ratio of cross-polarized channels compared with copolarized channels, these thermal noises are prevalent in cross-polarization SAR images, especially over the weak backscattering sea surface. Accurate radar calibration and specialized denoising schemes should be developed for every radar sensor mode to remove all these noises in cross-polarized SAR images. Sun and Li [53] proposed a method to improve the quality of Sentinel-1 extra-wide (S1-EW) mode cross-polarized image for sea ice monitoring. Similar algorithms should also be used in the future to eliminate the noise of Radarsat-2 ScanSAR images before using them to derive hurricane winds.

Furthermore, although the new model can effectively estimate the hurricane wind speed with the concise form of model function, two aspects need to be improved in our future works: 1) the selection of the tangential wind profile model in the asymmetric model. The M16 model does not perform well in the hurricane eye, limiting the wind estimation accuracy of the IMAHP model in the hurricane eye area and 2) the current asymmetry distribution mode based on the first azimuthal mode of asymmetry can only capture the asymmetric information in the direction of the strongest wind speed, while the description of the asymmetry in other directions is relatively inadequate.

VI. Conclusion

Cross-polarization SAR can provide high resolution and accurate sea surface wind observations of hurricanes. It gives us an opportunity to investigate the details of hurricane structure. In this article, an IMAHP model has been proposed to estimate the hurricane wind speed distribution. In the IMAHP model, we simplify the model function using the existing tangential winds model, and the cross-polarized SAR observations are selected to determine the model parameters. Comparisons with other existing hurricane models under different hurricane cases are presented. Statistical results show that the proposed IMAHP model performs better in capturing the asymmetric distribution of hurricane winds, and its simulation results are closer with airborne measurements.

In the future, we will try to improve the model results of the hurricane eye area and test the feasibility of implementing the proposed model in other spaceborne sensors.

Acknowledgment

The authors would like to thank the Canadian Space Agency for providing RADARSAT-2 dual-polarization SAR images, the NOAA Hurricane Research Division, NOAA Aircraft Operations Center, and the U.S. Air Force for collecting and maintaining the SFMR and dropwindsonde data.

References

[1] P. J. Vickery, F. J. Masters, M. D. Powell, and D. Wadhera, "Hurricane hazard modeling: The past, present, and future," *J. Wind Eng. Ind. Aerodyn.*, vol. 97, no. 7/8, pp. 392–405, 2009.

[2] B. Duan, W. Zhang, X. Yang, H. Dai, and Y. Yu, "Assimilation of typhoon wind field retrieved from scatterometer and SAR based on the Huber norm quality control," *Remote Sens.*, vol. 9, pp. 987–996, 2017.

[3] G. J. Holland, "An analytic model of the wind and pressure profiles in hurricanes," *Monthly Weather Rev.*, vol. 108, no. 8, pp. 1212–1218, 1980.

[4] X. Li *et al.*, "Tropical cyclone morphology from spaceborne synthetic aperture radar," *Bull. Amer. Meteor. Soc.*, vol. 94, pp. 215–230, 2013.

[5] W. Shao, X. Li, P. Hwang, B. Zhang, and X. Yang, "Bridging the gap between cyclone wind and wave by C-band SAR measurements," *J. Geophys. Res., Oceans*, vol. 122, pp. 6714–6724, 2017.

[6] A. Mouche, B. Chapron, J. Knaff, Y. L. Zhao, B. Zhang, and C. Combot, "Copolarized and cross-polarized SAR measurements for high-resolution description of major hurricane wind structures: Application to Irma category5 hurricane," *J. Geophys. Res., Oceans*, vol. 124, no. 6, pp. 3905–3922, 2019.

[7] X. Yang, X. Li, Q. Zheng, X. Gu, W. G. Pichel, and Z. Li, "Comparison of ocean-surface winds retrieved from QuikSCAT scatterometer and radarsat-1 SAR in offshore waters of the U.S. west coast," *IEEE Geosci. Remote. Sens. Lett.*, vol. 8, no. 1, pp. 163–167, Jan. 2011.

[8] X. Yang, G. Liu, Z. Li, and Y. Yu, "Preliminary validation of ocean surface vector winds estimated from China's HY-2A scatterometer," *Int. J. Remote Sens.*, vol. 35, no. 11/12, pp. 4532–4543, 2014.

[9] X. Zhou, J. Chong, X. Yang, W. Li, and X. Guo, "Ocean surface wind retrieval using SMAP L-Band SAR," *IEEE J. Sel. Top. Appl. Earth Observ. Remote Sens.*, vol. 10, no. 1, pp. 65–74, Jan. 2017.

[10] A. Stoffelen and D. Anderson, "Scatterometer data interpretation: Estimation and validation of the transfer function CMOD4," *J. Geophys. Res., Oceans*, vol. 102, no. C3, pp. 5767–5780, 1997.

[11] H. Hersbach, A. Stoffelen, and S. de Haan, "An improved C-band scatterometer ocean geophysical model function: CMOD5," *J. Geophys. Res., Oceans*, vol. 112, no. C3, 2007, Art. no. C03006.

[12] J. Verspeek, A. Stoffelen, M. Portabella, H. Bonekamp, C. Anderson, and J. F. Saldana, "Validation and calibration of ASCAT using CMOD5.n," *IEEE Trans. Geosci. Remote Sens.*, vol. 48, no. 1, pp. 386–395, Jan. 2010.

[13] A. Stoffelen, J. A. Verspeek, J. Vogelzang, and A. Verhoef, "The CMOD7 geophysical model function for ASCAT and ERS wind retrievals," *IEEE J. Sel. Top. Appl. Earth Observ. Remote Sens.*, vol. 10, no. 5, pp. 2123–2134, May 2017.

[14] H. Shen, Y. J. He, and W. Perrie, "Speed ambiguity in hurricane wind retrieval from SAR imagery," *Int. J. Remote Sens.*, vol. 30, no. 11, pp. 2827–2836, 2009, Art. no. Pii 912621193.

[15] X. Yang, X. Li, W. G. Pichel, and Z. Li, "Comparison of ocean surface winds from ENVISAT ASAR, MetOp ASCAT scatterometer, buoy measurements, and NOGAPS model," *IEEE Trans. Geosci. Remote Sens.*, vol. 49, no. 12, pp. 4743–4750, Dec. 2011.

[16] B. Zhang and W. Perrie, "Cross-polarized synthetic aperture radar: A new potential measurement technique for hurricanes," *Bull. Amer. Meteorol. Soc.*, vol. 93, no. 4, pp. 531–541, 2012.

[17] B. Zhang, W. Perrie, J. A. Zhang, E. W. Uhlhorn, and Y. He, "High-resolution hurricane vector winds from C-Band dual-polarization SAR observations," *J. Atmos. Ocean. Technol.*, vol. 31, no. 2, pp. 272–286, 2014.
[18] H. Shen, W. Perrie, Y. J. He, and G. Q. Liu, "Wind speed retrieval from VH dual-polarization RADARSAT-2 SAR images," *IEEE Trans. Geosci. Remote Sens.*, vol. 52, no. 9, pp. 5820–5826, Sep. 2014.
[19] J. Horstmann, S. Falchetti, C. Wackerman, S. Maresca, M. J. Caruso, and H. C. Graber, "Tropical cyclone winds retrieved from C-Band cross-polarized synthetic aperture radar," *IEEE Trans. Geosci. Remote Sens.*, vol. 53, no. 5, pp. 2887–2898, May 2015.
[20] H. Shen, W. Perrie, and Y. J. He, "Evaluation of hurricane wind speed retrieval from cross-dual-pol SAR," *Int. J. Remote Sens.*, vol. 37, no. 3, pp. 599–614, 2016.
[21] G. Zhang, X. Li, W. Perrie, P. A. Hwang, B. Zhang, and X. Yang, "A hurricane wind speed retrieval model for C-Band RADARSAT-2 cross-polarization ScanSAR images," *IEEE Trans. Geosci. Remote Sens.*, vol. 55, no. 8, pp. 4766–4774, Aug. 2017.
[22] G.-J. V. Zadelhoff, A. Stoffelen, P. W. Vachon, J. Wolfe, J. Horstmann, and M. B. Rivas, "Retrieving hurricane wind speeds using cross-polarization C-band measurements," *Atmos. Meas. Techn.*, vol. 7, pp. 437–449, 2014.
[23] A. A. Mouche, B. Chapron, B. Zhang, and R. Husson, "Combined co- and cross-polarized SAR measurements under extreme wind conditions," *IEEE Trans. Geosci. Remote Sens.*, vol. 55, no. 12, pp. 6746–6755, Dec. 2017.
[24] G. J. Holland, J. I. Belanger, and A. Fritz, "A revised model for radial profiles of hurricane winds," *Monthly Weather Rev.*, vol. 138, no. 12, pp. 4393–4401, 2010.
[25] A. C. Phadke, C. D. Martino, K. F. Cheung, and S. H. Houston, "Modeling of tropical cyclone winds and waves for emergency management," *Ocean Eng.*, vol. 30, no. 4, pp. 553–578, 2003.
[26] K. J. Mallen, M. T. Montgomery, and B. Wang, "Reexamining the near-core radial structure of the tropical cyclone primary circulation: Implications for vortex resiliency," *J. Atmos. Sci.*, vol. 62, no. 2, pp. 408–425, 2005.
[27] M. Sitkowski, J. P. Kossin, and C. M. Rozoff, "Intensity and structure changes during hurricane eyewall replacement cycles," *Monthly Weather Rev.*, vol. 139, no. 12, pp. 3829–3847, 2011.
[28] G. Zhang, B. Zhang, W. Perrie, Q. Xu, and Y. J. He, "A hurricane tangential wind profile estimation method for C-Band cross-polarization SAR," *IEEE Trans. Geosci. Remote Sens.*, vol. 52, no. 11, pp. 7186–7194, Nov. 2014.
[29] X. Zhou *et al.*, "Estimation of tropical cyclone parameters and wind fields from SAR images," *Sci. China Earth Sci.*, vol. 56, pp. 1977–1987, 2013.
[30] H. E. Willoughby, R. W. R. Darling, and M. E. Rahn, "Parametric representation of the primary hurricane vortex. Part II: A new family of sectionally continuous profiles," *Monthly Weather Rev.*, vol. 134, no. 4, pp. 1102–1120, 2006.
[31] V. T. Wood and L. W. White, "A new parametric model of vortex tangential-wind profiles: Development, testing, and verification," *J. Atmos. Sci.*, vol. 68, no. 5, pp. 990–1006, 2011.
[32] S. Wang, R. Toumi, A. Czaja, and A. V. Kan, "An analytic model of tropical cyclone wind profiles," *Quart. J. Roy. Meteorol. Soc.*, vol. 141, no. 693, pp. 3018–3029, 2015.
[33] P. L. N. Murty, P. K. Bhaskaran, R. Gayathri, B. Sahoo, T. S. Kumar, and B. SubbaReddy, "Numerical study of coastal hydrodynamics using a coupled model for Hudhud cyclone in the Bay of Bengal," *Estuarine Coastal Shelf Sci.*, vol. 183, pp. 13–27, 2016.
[34] L. J. Shapiro, "The asymmetric boundary-layer flow under a translating hurricane," *J. Atmos. Sci.*, vol. 40, no. 8, pp. 1984–1998, 1983.
[35] Y. Q. Wang and G. J. Holland, "Tropical cyclone motion and evolution in vertical shear," *J. Atmos. Sci.*, vol. 53, no. 22, pp. 3313–3332, 1996.
[36] P. D. Reasor, M. T. Montgomery, and L. D. Grasso, "A new look at the problem of tropical cyclones in vertical shear flow: Vortex resiliency," *J. Atmos. Sci.*, vol. 61, no. 1, pp. 3–22, 2004.
[37] B. W. Klotz and H. Jiang, "Examination of surface wind asymmetries in tropical cyclones. Part I: General structure and wind shear impacts," *Monthly Weather Rev.*, vol. 145, no. 10, pp. 3989–4009, 2017.
[38] Y. S. Chen and M. K. Yau, "Asymmetric structures in a simulated land-falling hurricane," *J. Atmos. Sci.*, vol. 60, no. 18, pp. 2294–2312, 2003.
[39] R. J. Ross and Y. Kurihara, "A simplified scheme to simulate asymmetries due to the beta-effect in barotropic vortices," *J. Atmos. Sci.*, vol. 49, no. 17, pp. 1620–1628, 1992.
[40] S. H. Houston, W. A. Shaffer, M. D. Powell, and J. Chen, "Comparisons of HRD and SLOSH surface wind fields in hurricanes: Implications for storm surge modeling," *Weather Forecasting*, vol. 14, no. 5, pp. 671–686, 1999.
[41] L. Xie, S. W. Bao, L. J. Pietrafesa, K. Foley, and M. Fuentes, "A real-time hurricane surface wind forecasting model: Formulation and verification," *Monthly Weather Rev.*, vol. 134, no. 5, pp. 1355–1370, 2006.
[42] J. D. McCalpin, "On the adjustment of azimuthally perturbed vortices," *J. Geophys. Res.*, vol. 92, no. C8, pp. 8213–8225, 1987.
[43] M. Olfateh, D. P. Callaghan, P. Nielsen, and T. E. Baldock, "Tropical cyclone wind field asymmetry—Development and evaluation of a new parametric model," *J. Geophys. Res., Oceans*, vol. 122, no. 1, pp. 458–469, 2017.
[44] E. W. Uhlhorn and P. G. Black, "Verification of remotely sensed sea surface winds in hurricanes," *J. Atmos. Ocean. Technol.*, vol. 20, no. 1, pp. 99–116, 2003.
[45] E. W. Uhlhorn, P. G. Black, J. L. Franklin, M. Goodberlet, J. Carswell, and A. S. Goldstein, "Hurricane surface wind measurements from an operational stepped frequency microwave radiometer," *Monthly Weather Rev.*, vol. 135, no. 9, pp. 3070–3085, 2007.
[46] T. F. Hock and J. L. Franklin, "The NCAR GPS dropwindsonde," *Bull. Amer. Meteorol. Soc.*, vol. 80, no. 3, pp. 407–420, 1999.
[47] G. S. Zhang, W. Perrie, X. F. Li, and J. A. Zhang, "A hurricane morphology and sea surface wind vector estimation model based on C-Band cross-polarization SAR imagery," *IEEE Trans. Geosci. Remote Sens.*, vol. 55, no. 3, pp. 1743–1751, Mar. 2017.
[48] G. M. Barnes, "Atypical thermodynamic profiles in hurricanes," *Monthly Weather Rev.*, vol. 136, no. 2, pp. 631–643, 2008.
[49] M. D. Powell, S. H. Houston, L. R. Amat, and N. Morisseau-Leroy, "The HRD real-time hurricane wind analysis system," *J. Wind Eng. Ind. Aerodyn.*, vol. 77/78, pp. 53–64, 1998.
[50] G. Zhang, X. Li, W. Perrie, B. Zhang, and L. Wang, "Rain effects on the hurricane observations over the ocean by C-band synthetic aperture radar," *J. Geophys. Res., Oceans*, vol. 121, no. 1, pp. 14–26, 2016.
[51] B. W. Klotz and E. W. Uhlhorn, "Improved stepped frequency microwave radiometer tropical cyclone surface winds in heavy precipitation," *J. Atmos. Ocean. Technol.*, vol. 31, no. 11, pp. 2392–2408, 2014.
[52] H. Shen, C. Seitz, W. Perrie, Y. J. He, and M. Powell, "Developing a quality index associated with rain for hurricane winds from SAR," *Remote Sens.*, vol. 10, no. 11, 2018, Art. no. 1783.
[53] Y. Sun and X. Li, "Denoising Sentinel-1 extra-wide mode cross-polarization images over sea ice," *IEEE Trans. Geosci. Remote Sens.*, to be published, doi: 10.1109/TGRS.2020.3005931.

Sheng Wang received the B.S. degree in remote sensing science and technology from Wuhan University, Wuhan, China, in 2017, and the M.S. degree in electronic and communication engineering from the Aerospace Information Research Institute, Chinese Academy of Sciences (CAS), Beijing, China, in 2020. He is currently working toward the Ph.D. degree in civil engineering at the University of Macau, Macau, China.

His current research interests include the application of machine learning in ocean remote sensing.

Xiaofeng Yang (Senior Member, IEEE) received the B.S. degree in environmental science from Sichuan University, Chengdu, China, in 2005, and the Ph.D. degree in cartography and geographic information systems from the Institute of Remote Sensing Applications (IRSA), Chinese Academy of Sciences (CAS), Beijing, China, in 2010.

From 2009 to 2010, he was a Visiting Research Scientist with the Department of Atmospheric and Oceanic Science, University of Maryland, College Park, MD, USA. In 2010, he joined IRSA, CAS, and he was promoted to an Associate Professor, in 2013 and a Full Professor, in 2016. His research interests include satellite oceanography, synthetic aperture radar image processing, and marine atmospheric boundary layer process studies.

Dr. Yang is an Associate Editor for *Remote Sensing* (MDPI) and an Editorial Board Member for the IEEE TRANSACTIONS ON GEOSCIENCE AND REMOTE SENSING. He is also the Secretary-General of the Technical Committee on Earth Science from Space, Chinese Society of Space Research.

Haiyan Li received the B.S. degree in physics from HeBei Normal University, Shijiazhuang, China, in 1999, the M.S. degree in physics oceanography from the Ocean University of China, Qingdao, China, in 2004, and the Ph.D. degree in physics oceanography from the Institute of Oceanology, Chinese Academy of Sciences, Qingdao, China, in 2007.

In 2007, she joined the University of Chinese Academy of Sciences, Beijing, China, where she is currently an Associate Professor. Her research interests include oceanic microwave remote sensing, particularly in the field of air–sea interactions, ocean dynamic process study, and target detection by advanced synthetic aperture radar (SAR), such as polarized SAR and compact polarimetry SAR.

Kaijun Ren received the B.S degree in applied mathematics and the M.S. and Ph.D. degrees in computer science from the National University of Defense Technology, Changsha, China, in 1998, 2003, and 2008, respectively.

He is currently a Professor with the College of Computer and College of Meteorology and Oceanography, National University of Defense Technology, China. His current research interests include high-performance computing, cloud computing, big data, and their interdisciplinary applications in ocean science and meteorology.

Xiaobin Yin (Senior Member, IEEE) received the B.Sc. and Ph.D. degrees in ocean science and physical oceanography from the Ocean University of China, Qingdao, China, in 2003 and 2007, respectively, studying the remote sensing of sea surface salinity and sea surface wind with multifrequency microwave radiometers.

From 2009 to 2015, he was involved in the validation of the SMOS L-band radiometric measurements and the improvement of the European Space Agency Level 2 ocean salinity retrieval algorithms with the Laboratoire d'Oceanographie et du Climat—Experimentation et Approches Numeriques, Paris, France. From 2015 to 2016, he was a Research Professor with the National Space Science Center, Chinese Academy of Sciences (CAS), Beijing, China, and was involved in the pre-research of the SSS space mission of China. He is currently a Research Professor with Piesat Information Technology Company Ltd., Beijing, China, a high-tech enterprise that specializes in the study and application of satellite technology. He is also an Adjunct Professor with the Ocean University of China and Hohai University, Nanjing, China.

Die Hu received the B.S. degree in geographic information science from the China University of Geosciences (Beijing), Beijing, China, in 2017. She is currently working toward the Ph.D. degree in cartography and geographic information systems with the Aerospace Information Research Institute, Chinese Academy of Sciences (CAS), Beijing, China.

Her current research interests include the application of thermal infrared remote sensing in urban environment evaluation.

Yanlei Du (Member, IEEE) received the B.S. degree in remote sensing science and technology from Chang'an University, Xi'an, China, in 2014, and the Ph.D. degree in cartography and geographic information systems from the Institute of Remote Sensing and Digital Earth (RADI), Chinese Academy of Sciences (CAS), Beijing, China, in 2019.

During the Ph.D. program (2017–2019), he was a Visiting Scholar with the Department of Electrical Engineering and Computer Science (EECS), University of Michigan, Ann Arbor, MI, USA. He is currently a Postdoctoral Research Fellow with the Department of Electronic Engineering, Tsinghua University, Beijing, China. His research interests include computational electromagnetics in applications of ocean remote sensing and satellite oceanography.